Chapter 7
Test Methods

Standard Test Procedures for Relevant Material Properties for Structural Analysis

Gerald G. Trantina and Joseph T. Woods
General Electric Corporate Research and Development, Schenectady, NY 12301, USA

INTRODUCTION

Engineering thermoplastics exhibit complex behavior when subjected to constant, increasing, or cyclic mechanical loads. As these materials begin to be used more in load-bearing designs, engineers must be able to predict the structural performance of actual molded parts. However, the necessary material properties to do this are usually not available. While standard data sheet properties can be useful for initial material selection, they are inadequate to predict the structural performance of a part. And even when the necessary engineering data exist, they are usually not measured at the same time, strain rate, temperature, or stress as those of a particular application. The structural analyst's task is to predict the performance of a design at end-use conditions in terms of both operating temperature and loading (constant, increasing, or cyclic). To do this, two types of information are required: data to perform structural analysis calculations and data to assess performance. The material properties required for structural analysis of thermoplastic components will be presented. The shortcomings of data sheet data will be overcome with standard test procedures that provides relevant material properties for structural analysis.

There is a significant amount of activity focused on developing standards for plastic materials test data. Certainly, inconsistent test procedures and material data reduce the credibility of the plastics industry. Adoption of uniform international standards will address this problem. However, to the design engineer, the usefulness of the data is also extremely important. If the data is dependent on the test specimen geometry or the type of loading, it cannot be used to predict part performance. Issues that will be addressed in this paper

include the stiffness and strength of fiber-filled materials, ductile-brittle behavior of unfilled materials and time-dependent material behavior. This material behavior will be described in the context of how the data is used to predict structural performance of parts. For the design engineer, relevant material properties are the key to successful thermoplastic applications with short product development times.

STIFFNESS AND STRENGTH

An accurate characterization of the strength and stiffness of glass-filled thermoplastics is necessary to predict the strength and stiffness of components that are injection molded with these materials. The mechanical properties of glass-reinforced thermoplastics are generally measured in tension using end-gated, injection-molded ASTM Type I (dog-bone) specimens. However, the gating and the direction of loading of these molded specimens yields nonconservative stiffness and strength results due to the high axial orientation of glass fibers that occurs in the direction of flow (and loading) during molding.

Previous studies[1,2] have shown that injection-molded, glass-reinforced thermoplastics are anisotropic values of stiffness and strength in the cross-flow direction are substantially lower than in the flow direction. The tensile stiffness and strength were measured by using dog-bone specimens that were cut in both the flow and cross-flow direction from edge-gated plaques of various thicknesses. The cross-flow tensile modulus and strength of 30% glass-filled materials is approximately 60% of the flow properties. Table 1 illustrates this for tensile and flexural strength. However, before the issues of predicting part strength need to be addressed, the part must be designed for stiffness.

Table 1. Average tensile and flexural strength of 152 x 381 x 3 mm fan-gated plaques

Material	Testing direction	Tensile strength, MPa	Flexural strength, MPa	Flexural/tensile strength ratio
PBT + 30% glass fiber	Flow Cross-flow	125 71	119 111	1.59 1.56
PC + 30% glass fiber	Flow Cross-flow	122 78	194 114	1.59 1.46
PPO/PA + 30% glass fiber	Flow Cross-flow	143 92	209 108	1.46 1.17
PA + 33% glass fiber	Flow Cross-flow	169 96	236 120	1.40 1.25

Table 1. Average tensile and flexural strength of 152 x 381 x 3 mm fan-gated plaques

Material	Testing direction	Tensile strength, MPa	Flexural strength, MPa	Flexural/tensile strength ratio
PC + 15% glass fiber	Flow Cross-flow	87 68	130 102	1.49 1.50
PPO/PA + 10% glass fiber	Flow Cross-flow	84 80	110 101	1.31 1.26

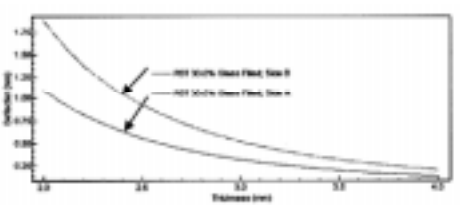

Figure 1. 30% glass-filled PBT plate (50 cm x 25 cm) deflection versus thickness for edge gates with orthotropic analysis and isotropic analysis with flow modulus (data sheet).

A simple example of part stiffness for fiber-filled materials is shown in Figure 1. Structural stiffness is dependent on material properties, part geometry and for fiber-filled materials, the gate location - where the polymer enters the mold. In Figure 1 the deflection of a 50 cm (side A) by 25 cm (side B) rectangular plate is shown as a function of plate thickness. The plate is loaded with a pressure of 0.5 kPa and is fixed on all four sides. The material is a 30% glass-filled PBT. The upper curve is for a plate with an edge gate on side B and the lower curve for a plate with and edge gate on side A. The linear structural analysis is performed with a standard orthotropic material model.[1] It should be noted that the plate is stiffer with the gate on the long side (side A) since the short side (25 cm) controls the plate deflection and the flow direction and the stiffest material behavior is in the short side direction. Also, an isotropic analysis would produce a nonconservative, erroneous result. For example, for a 3 mm thick plate, the plate deflection for a side B gated plate is 0.52 mm and for a side A gated plate is 0.32 mm (Figure 1) using an orthotropic analysis while the deflection using an isotropic analysis with the flow direction modulus (data sheet) would be 0.26 mm (a 19% error compared to the optimum gate A configuration).

Next, the strength of parts molded with glass-filled materials must be considered. While this is a complex failure analysis problem that is beyond the scope of this paper, an important observation about the relationship of the tensile strength to the flexural strength should be noted. For unfilled materials, the tensile strength is 2/3 of the flexural strength. This relationship holds because the procedure for computing the flexural strength is elastic and does not account for the fully plastic behavior of the bending test. A simple accounting for this plastic behavior produces a factor of 2/3 to be multiplied times the simple elastic

beam bending equation. Reference 3 provides the mathematical and mechanical justification of this 2/3 factor. This is validated by noting that for over 800 unfilled resins the flexural strength is 1.56 times the tensile strength.[3] Thus, the design engineer should use the tensile strength or multiply the flexural strength by 2/3.

For fiber-filled materials there is a significant reduction in the ductility with strains-to-failure of 3-4% versus roughly 100% for unfilled materials. However, the matrix resin can achieve very large strains and significant plasticity even though the overall strains may be only 3-4%. Also, the stress-strain curves become nearly flat prior to failure indicating gross plastic behavior. Therefore the same mechanics concepts applied to unfilled resins[3] might be applied to fiber-filled resins. Table 1 summarizes the ratio of the flexural to the tensile strength of six resin/fiber systems. The average ratio is 1.42. Thus, there is substantial evidence that the tensile strength rather than the flexural strength should be used for failure predictions of parts molded from fiber-filled materials or the flexural strength should be multiplied by 2/3. However, as mentioned earlier, the details of the failure prediction method is complex[1] and is beyond the scope of this paper.

DUCTILE-BRITTLE IMPACT

The design engineer is continually challenged to predict part performance under high loading rates and sometimes low temperatures. Of particular concern is the identification of combinations of stress state, strain-rate and temperature that lead to brittle part failure. It is well-known that triaxial stress states created by notches, holes, fillets and thick sections increase the potential of brittle failure. Unfortunately there are no simple methods to predict brittle failure of thermoplastic parts. Standardizing on the Charpy or Izod impact test is not going to improve this situation.[3] However, there are new approaches useful to the design engineer.[4]

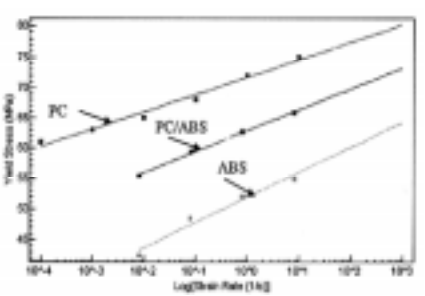

Figure 2. Yield stress at room temperature versus strain rate for PC, PC/ABS and ABS.

Most unfilled engineering thermoplastics exhibit ductile behavior in tensile tests with increasing strength as strain rate increases (Figure 2) and/or temperature decreases. However, parts typically have complex geometry with local areas of triaxial stress states. The controlled testing of notched beams with various notch radii and beam thicknesses, where the load-displacement response is measured for various loading rates and temperatures, provides useful information for a failure criteria for plastic parts.[4] These tests also illustrate the extremely limited usefulness of Izod or Charpy impact tests.

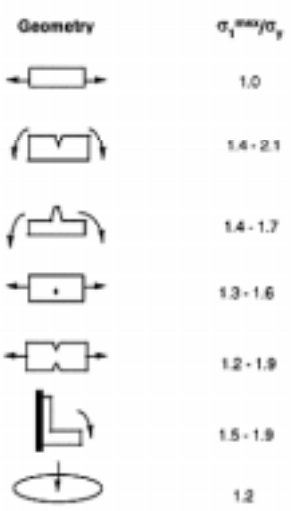

Figure 3. Geometric severity ratios for typical part features.

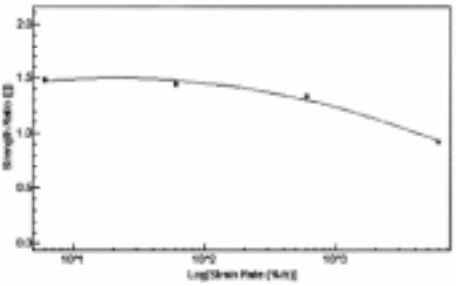

Figure 4. Strength ratio versus strain rate for PBT at -30°C.

Geometries producing tensile, triaxial stress states having a large maximum principal stress components are more susceptible to brittle failure. If brittle failure is a possibility for the material, then the actual stress state produced within the part and the material's failure criterion must be considered. One way of characterizing the susceptibility of a geometry to brittle failure is to numerically calculate the geometry's peak maximum principal stress level and divide it by the yield stress of the material. This ratio is referred to as the "geometric severity ratio." Since the geometric severity ratio normalizes the peak, maximum principal stress level in the geometry by the yield stress of the material used in the analysis, it represents a purely geometric factor. Note that the geometric severity ratio corresponds to a worst case loading condition, i.e., a load level that results in the maximum possible level of maximum principal stress in the part assuming elastic-perfectly plastic material behavior. Geometries having larger geometric severity ratios are more likely to fail brittlely. Figure 3 provides a list of geometric severity ratios for common, generic geometries. In many geometries, local stress levels will be affected by geometric parameters such as radius, thickness, etc. For these geometries a geometric severity ratio range is provided. Using Figure 3 geometric severity ratios can be chosen which represent features of the part being designed. These geometric severity ratios can then be compared to a strength ratio, the material's critical maximum principal stress to yield stress ratio, i.e., its failure criterion, at the appropriate rate and temperature (Figure 4) to determine if brittle failure is possible for an arbitrarily high structural load. If brittle failure is a possibility, then maximum principal stress levels must be kept below those required to initiate failure by adjusting local geometric parameters or by limiting the loading on the structure.

TIME AND TEMPERATURE DEPENDENT DEFORMATION

For the design engineer, the purpose of measuring time-dependent deformation is to obtain useful information that can then be used to predict time-dependent part performance.[5] The

important consideration here is the type of loading-tension versus flexure and constant load versus constant displacement. In the creep test, a specimen is rapidly loaded and then the load is held constant at a constant temperature. For a tensile specimen, the strain should be measured with an extensometer in the gauge section where the stress is uniform. For the stress relaxation test, the specimen is rapidly loaded and then the displacement or strain is held constant. The creep test is more common and probably simpler since dead weight loading can be used with multiple creep stations. The uniaxial tensile test is considered most useful for producing accurate, consistent results that can be easily interpreted. An extensometer is used to measure uniform strain accurately, and the stress is uniform and equal to the load divided by the specimen's net-section area.

Flexural (bending) creep tests have been widely used with polymers. However, in the flexural test, linear-elastic, time-independent beam equations are used to calculate the bending stress using the applied load. Unfortunately, because of the time-dependent, nonlinear, stress-strain response of thermoplastics, the simple bending equations are often inadequate. Constant stress is not maintained because of stress redistribution - the stress distribution is not linear through the thickness of the beam.

The heat deflection temperature (HDT) is a common measure of heat resistance in the plastics industry. Such a test, which involves variable temperature and arbitrary stress and deflection, is of no use in predicting the structural performance of a thermoplastic at any temperature, stress, or time. In addition, it can be misleading when comparing materials. A material with a higher HDT than another material could exhibit more creep than the other material at a lower temperature. For purposes of predicting part performance and for material selection, tensile creep data is the desired measurement.

Since load-bearing applications are designed for stiffness and strength, time-strain data are not directly useful. However, a curve-fitting interpretation of these data that retains the important features common to many of the creep models - log-time representation and Arrhenius relations for temperature - is useful to the design engineer. In this section, the steps required to translate the initial strain-time data to an isochronous stress-strain curve for any time or temperature will be described.

Several methods for fitting and extrapolating time-strain data could be used. The objective should be to obtain the most accurate fit while achieving reasonable extrapolation predictions with minimum complexity. It has been determined based on visual inspection, that a second-order polynomial function in log time can be used where:

$$\varepsilon_t = A(\log t)^2 + B(\log t) + C$$

The constants are determined by a least-squares curve-fitting method. An example for a PC/ABS blend tested at 10.3 MPa and 50^{o}C is shown in Figure 5. Engineering judgment must be used concerning the appropriate extrapolation in time. Caution should be exercised

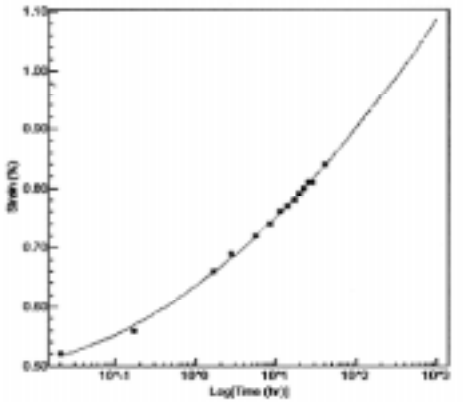

Figure 5. Strain versus time for PC/ABS with a constant stress of 10.3 MPa and temperature of 50°C.

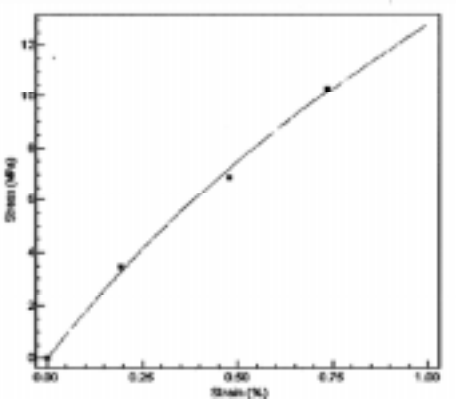

Figure 6. Isochronous stress-strain curve for PC/ABS at 40°C and 100 hours.

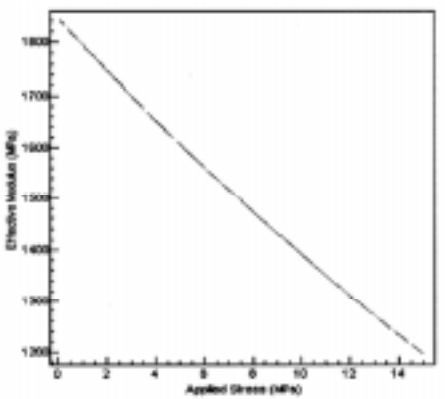

Figure 7. Effective modulus versus stress for PC/ABS at 40°C and 100 hours.

when more than one order of magnitude of time extrapolation is used.

Based on fundamental principles for thermally activated processes, use of the Arrhenius relation is reasonable to interpolate and extrapolate with temperature. Plotting the strains versus temperatures for a particular time and stress on a natural logarithm (ln) of strain versus the inverse of the absolute temperature graph results in a linear interpolation or extrapolation based on the Arrhenius relation.

Finally, the isochronous stress-strain curve is produced by choosing the appropriate temperature and plotting the stress-strain points taken from the Arrhenius plots at that temperature and the previously chosen time. For example, for the PC/ABS blend for 100 h and a temperature of 40°C, the isochronous stress-strain curve is produced (Figure 6).

For constant stress applications, the isochronous stress-strain curve can be used with standard equations by choosing the appropriate "effective modulus" considering the range of stresses in the application. This requires engineering judgment where higher stressed parts would typically be analyzed with a lower "effective modulus." For example, Figure 7 shows the effective modulus calculated from the isochronous stress-strain curve (Figure 6)

as the secant modulus. The use of this modulus based on the maximum stress in the part should provide a conservative estimate of the time and temperature dependent deflection of the part. When the isochronous stress-strain curve is highly nonlinear or the part geometry is complex, finite-element structural analysis techniques can be used. Then, the complete nonlinear, isochronous stress-strain curve can be used in a nonlinear finite-element analysis or a linear effective modulus can be used in a linear analysis.

CONCLUSIONS

Uniform standards for measuring mechanical properties of plastics will lead to consistent test data. However, for the design engineer, the usefulness of the data in predicting part performance is also very important. If the data is dependent on test specimen geometry or the type of loading, it cannot be used to predict component behavior. Data reported for flexural strength of unfilled and fiber-filled thermoplastics is about 50% greater than the tensile strength. This is simply a miscalculation of the flexural strength since elastic beam equations are used for the nearly fully plastic behavior of thermoplastics. The proper flexural strength calculation would be 2/3 times the elastic beam equation. The flexural strength would then be about the same as the tensile strength. Also, gate location and its effect on part deflection for fiber-filled materials can be treated with an orthotropic stress analysis. Izod and Charpy impact tests are simply two different beam bending loads (cantilever and 3-point bending) yielding single-point information. To predict ductile/brittle behavior of parts, geometry can be captured with a geometric severity factor and compared to the strength ratio - the material's critical maximum principal stress at the appropriate strain rate and temperature divided by the yield stress. Creep data displayed as "effective modulus" graphs provide useful geometry-independent design information for situations where time and temperature are important. HDT is simply a geometry and loading dependent temperature that is not useful for design purposes. The plastics industry must strive to develop standard mechanical tests that are independent of specimen geometry and thus useful to the design engineer who is responsible for part performance.

REFERENCES

1 Ambur, G. and Trantina, G., "Structural Failure Prediction with Short-Fiber Filled, Injection Molded Thermoplastics," Society of Plastics Engineers, 1988 ANTEC Conference Proceedings, pp. 1507-1511.

2 Stokes, V.K., Inzinna, L.P., Trantina, G.G., Liang, E.W., and Woods, J.T., "Mechanical Properties of Long-Fiber Filled Injection-Molded Thermoplastic Composites," 1994 ANTEC Conference Proceedings.

3 Trantina, G.G. and Oehler, P.R., "Standardization - Is It Leading to More Relevant Data for Design Engineers," 1994 ANTEC Conference Proceedings.

4 Woods, J.T. and Nimmer, R.P., "Design Aids for Preventing Brittle Failure in Polycarbonate and Polyetherimide," 1996 ANTEC Conference Proceedings.

5 Trantina, G.G. and Nimmer, R.P., **Structural Analysis of Thermoplastic Components**, *McGraw-Hill*, New York, 1994.

Factors Affecting Variation in Gardner Impact Testing

Mark Lavach
Elf Atochem North America

INTRODUCTION

Previous work[1] concluded that the Gardner Impact Test is useful to find the MFE for brittle thermoplastics such as acrylic and HIPS with standard deviations between 8% and 10%. Standard deviations of 15% were found for more ductile materials such as ABS or PC. Major sources of variation included the mounting of the apparatus (floor vs. bench), material quality, test temperature, and the operators' definition of failure. In an independent study,[2] Paxon Polymer found that testers mounted on standard laboratory benchtops yielded higher MFE's than those bolted directly to the floor. We have also observed that standard laboratory bench tops can crack after repeated use of the tester. This could seriously compromise the accuracy and precision of the test. More recently, the Vinyl Siding Institute (VSI) in their exhaustive round robin testing using PVC siding found residual standard deviations on the order of 15%.[3]

In a series of recent tests, we examined the effect of supporting table mass on the MFE of embossed and non-embossed PVC siding, along with several other typical thermoplastics. We hypothesized that the heavier supporting tables would absorb less impact energy due to less flexural or compressive deflection of the supporting table. The net result would be a decrease in the samples' MFE. Further, we believed that the precision of the test could be improved. Additionally, we looked into the effect of reducing the drop height increments to increase the test's precision.

EXPERIMENTAL

In many installations, the Gardner Tester is bolted to a table facilitating operation of the equipment by placing the equipment at an ergonomically friendly height. In our labs, we studied the effect of bolting the tester to tables of varying weight, ranging from 57 lbs to 440 lbs. The 57 lb table had a wooden top with steel frame supports. Heavier tables were constructed entirely of wood and could best be described as "butcher block" tables. These tables were not bolted to the floor. The testers were also fixed to the floor in an attempt to represent a supporting table of infinite mass. Initial studies were performed by a single operator

using non-embossed PVC siding sourced from a single box. Siding was cut into 2"x2" squares, and always taken from the same siding panel location. This material would also be used in all subsequent testing and as a control in tests involving other materials. MFE's were calculated using the Bruceton Staircase or "Up and Down" method.[4] Twenty samples were used for each calculation. Tests were run in pass/fail mode, and no attempt was made to find the brittle/ductile transition point for each of the plastics. Additionally, 20 samples were run for each test configuration to allow us good approximation for the test's starting point. Total variability studies incorporated 3 different operator teams who ran duplicate tests (20 samples per test) using two different testers on the three different tables.

RESULTS AND DISCUSSION

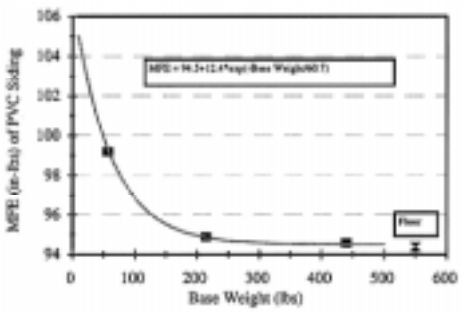

Figure 1. MFE vs. base weight (single operator).

Figure 1 shows results from a single operator test of non-embossed PVC siding. These results a fall off in the siding's MFE with increasing table mass. Statistical analysis of the data suggests that MFEs obtained using the 57 lb table were significantly different from those obtained with the 440 lb table. Both the floor supported and 440 lb table supported testers gave similar results. Twenty tests (400 samples) were then replicated on the 440 lb table to determine test variation. Using this test design, we found variation in the MFE of the tested siding to be about 11%. Variation in the MFE was not reduced during the testing cycle indicating that prior knowledge about the test's starting point had no influence on reducing overall test variation.

Differences in failure type classification by test operators could be an important source of test variation. Using the same non-embossed siding, we selected 3 teams of operators who ran duplicate tests on each of the three tables using two different testers. For this study, sample thickness variation was less than 2% of the mean thickness which should have minimal impact on test results. Using an ANOVA (Analysis of Variance) based experimental design, we could not only determine differences in supporting table results, but also look at differences between the operator teams and test equipment. Interactions, significant differences, and test variation could also be evaluated. Mean Failure Energy results are shown in Figure 2, where once again our initial hypothesis was supported: that is, increasing supporting table mass decreases a sample's MFE. Differences in MFEs between the lightest and heaviest tables were again considered statistically significant. Differences between the 440 lb table and the floor were considered statistically insignificant.

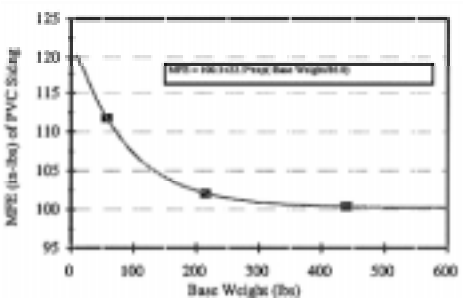

Figure 2. MFE vs. base weight (multiple operator).

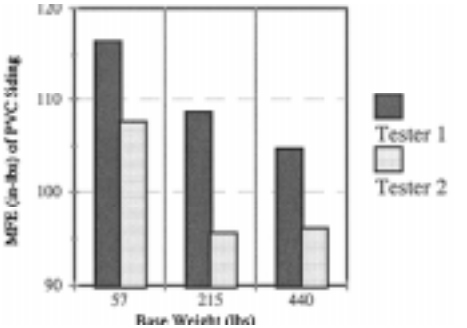

Figure 3. Gardner test equipment bias.

Table 1. Tup and weight effects

Table wt, lbs	Tup #	Weight #	MFE, in-lbs
215	1	1	120.9
215	1	2	118.5
215	2	1	97.5
215	2	2	96.3
440	1	1	114.9
440	1	2	112.9
440	2	1	98.0
440	2	2	96.5

Use of ANOVA based analysis also allowed us to investigate other contributions to variations in MFE determinations. While base mass was found to have the greatest effect on MFE, statistically significant differences were found between the two testers and the three different operator teams. There was significant equipment bias between the two testers (Figure 3). Mass measurements of both the tup and falling weight showed only small differences between the items. Falling weight guides were of identical radius, and there appeared to be no interference in the guides. Using the two heaviest tables (215, 440 lbs), tups and weights were exchanged between the two testers. This testing revealed that use of one tup repeatedly resulted in lower MFEs regardless of other equipment changes. This indicated that the equipment bias was correlated to differences in the tup (Table 1). Both tups had smooth, round surfaces of similar radii. Higher MFEs were found with the older of the two tups, which could be a result of strain hardening in the tup. Differences in MFEs obtained by the various teams were also found. One team consistently observed lower MFEs than the two other teams. These results confirm the SPI findings that failure identification differences between operators can influence test results.

We also looked at the effect of the various test variables (table, team, and tester) on the residual standard deviation of the test. Residual standard deviation (RSD), or coefficient of variation (COV), is defined as the mean divided by the standard deviation,[5] and is useful for comparing means of different magnitudes, units, or test conditions. RSD normalizes the standard deviation allowing for quick comparisons of variation over a wide range of test conditions and impact strengths. Using ANOVA based analysis we found the residual standard deviation to be independent of the tests' controlled variables (table, team, tester). Residual standard deviations from these tests were well in line with the estimated test variation observed in the single operator control studies.

Following these tests we evaluated the effects of supporting table mass on the MFE of embossed PVC siding. Embossed siding, which helps simulate a woodgrain appearance in PVC, also introduces an impact "flaw" into the siding surface. This flaw acts as a stress concentrator similar to a notch in a pendulum impact test. In general, the net result is a reduction in the part's impact resistance. For the samples, we quantified the depth of the embossing pattern in an attempt to measure its' effect on the test. In limited testing, we could not directly quantify the effects of embossing on impact resistance. More samples would be needed for a quantifiable determination. However, increasing base mass again reduced all of the sample MFEs. For one sample the effect was not only significant, but resulted in the sample's MFE falling below the 60 in-lb minimum standard for PVC siding.[6] Differences were not only significant, but also important. Too often we talk of test differences as being statistically significant, but offer no opinion on their relative importance.

Table 2. Effect of Base Weight on Thermoplastic MFE

Plastic	Supplier	Tup type	Supporting Base Weights, MFE (in-lbs)		
			57 lbs	215 lbs	440 lbs
ABS		C.125	273	256	246
HDPE		C.125	190	185	184
HIPS		C.125	179	164	170
PP (0.077")	A	H.250	121	120	110
PP(0.121")	B	C.125	196	185	184
PVC		H.250	112	102	101

We also tested a variety of other plastics. For these materials, 2 inch disks of each polymer were used in testing. Samples were prepared via injection molding. For stronger samples a conical tup was used. For all polymers similar trends regarding sample MFE vs. base mass were observed (Table 2). Once again, differences between the floor supported and the 440 lb tester were found to be insignificant. While increasing base mass reduced a sample's MFE, it had no effect on the residual standard deviation found in the test. Test variation was independent of the supporting table mass. Variation also appeared to be independent of a samples MFE. Tough materials exhibited similar residual standard deviations to brittle ones (Table 3). In general, an operator's familiarity with the test specimen had little impact on test variation. PVC, which we test regularly in our labs, appeared in the middle of total test variation. To reduce operator variation in failure determinations, careful inspection of some samples with either water or a stainable dye is recommended. Finally, we evaluated the influence of drop height increments on test variation with the 440 lb table. Our Gardner test tower is equipped with 8 in-lb (1") increments. For samples of known MFE, reduction of the drop height increment from 8 in-lb to 4 in-lb (0.5") increments significantly reduced a tests total variation (Table 4). Further reductions in the test increments are not likely to be as beneficial as one could begin to over-control the test. The Bruceton Staircase calculation requires somewhat robust changes in energies to be effective. Minimization of these changes could impact the calculation's ability to predict a sample's MFE. Ability to accurately place the falling weight at 2 in-lb (0.25") increments with an 8 lb. falling weight is also debatable.

Table 3. Variation in Gardner Test Results

Plastic	Test size	Ave. RSD	Std. Dev., in-lbs
ABS	21	5.2	2.8
HDPE	21	4.1	2.0
HIPS	21	9.4	6.4
PP (0.077")	21	10.7	6.6
PP (0.121")	21	7.9	6.0
PVC	21	9.1	3.9

Table 4. Effect of Drop Height Increments on PVC MFE and RSD

Increment size, in-lbs	Cases	MFE, in-lbs	RSD, %
4	21	99.2	3.4
8	24	95.5	4.8

CONCLUSIONS

We have shown that providing a solid, rigid support with increasing mass will lower a sample's MFE. Heavy, rigid bases have less deflection and compression than lighter ones. resulting in more energy transferal to the sample during the impact event. Based on statistical analysis, this table should weigh more than 400 lbs and be constructed in a fashion which eliminates possible deflection and compression of the support. The test can also be subject to significant equipment bias, with different testers giving different results. For pass/fail determinations, operator interpretation of failure could also result in differences in sample MFEs. We would expect that the magnitude of variation would increase for determinations of the brittle/ductile transition point. Increasing base mass had no impact on test variation. However reducing drop height increments reduced the overall test variation. Overall test variation appeared independent of impact energy.

ACKNOWLEDGMENTS

The author wishes to thank Elf Atochem North America for its support while conducting this project. Special thanks are given to personnel who participated in the drop testing of the samples as well as to BASF, Dow Chemical, Paxon Polymer Company, Exxon Chemicals and the Vinyl Siding Institute (VSI) who supplied samples for testing.

REFERENCES

1 SPI/SPD Technical Committee Report, Sheet Producers Division, "Recommended Guidelines for the Standardized Use of the Test Method Described in ASTM D-3029-82 for Determining the Relative Impact Resistance of Custom Extruded Sheet.", April 1994.

2 Paxon Polymer Company, Private Communication.

3 Vinyl Siding Institute Final Report, "Gardner Impact Round Robin Test Program", June 1997.

4 Brownlee, K.A., Hodgest, J.L.,Jr., and Rosenblatt, Murray, "The Up and Down Method with Small Samples," *American Statistical Association Journal*, Vol **48**, 1953, pp 262-277.

5 Havlicek, L.L., Crain, R.D., "**Practical Statistics for the Physical Sciences**", *American Chemical Society*, Washington, DC., 1988, pp.77-78.

6 ASTM D-3679, "Standard Specification for Rigid Poly(Vinyl Chloride)(PVC) Siding." Annual Book of ASTM Standards, Vol 8.02.94.

Radiation Resistance of Multilayer Films by Instrumented Impact Testing

Robert Wojnarowski, Michael T. K. Ling, Atul Khare, and L. Woo
Baxter International, Round Lake, IL 60073, USA

INTRODUCTION

In the medical packaging industry, multilayer films are frequently used for a multitude of applications ranging from primary sterile fluids containers to secondary and tertiary protective packaging. Also, terminal sterilization by ionizing radiation has steadily gained popularity for its effectiveness and simplicity. However, frequently material degradations also accompany the sterilization process. This is due to the depletion of antioxidants during and after the irradiation step. In addition, many of the material degradation processes continue long after the radiation treatment. This is due to actions of long lasting free radicals, peroxy and hydroperoxides created during irradiation, as they continue to react with atmospheric oxygen diffusing in from the external of the packaging to propagate the oxidative chain reaction. In this article we will present the development of a radiation resistant multi-layer film with the aid of an instrumented impact tester where material degradation can be quantified.

RADIATION DEGRADATION OF POLYMER FILMS

Figure 1. Compton scattering with matter.

Both the sterilizing action and the degradation caused by ionizing radiation are believed to result from Compton secondary electrons from the primary interaction event. The high energy gamma photon or accelerated electrons (from the e-Beam source) first interact with the atom in the material being irradiated, creating a secondary high energy electron and a recoiling photon or electron, with reduced energy compared with the incoming beam. The cascade is propagated until all the excess energy above the ionization threshold is dissipated. Thus, from a single incoming photon or electron, a shower (Figure 1) of secondary electrons is generated and they are responsible for the bio-burden kill and material degradation.[1]

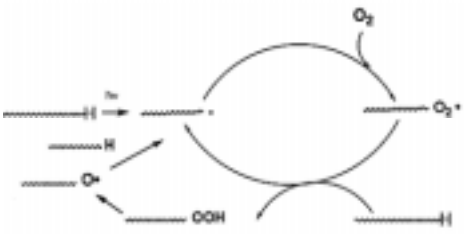

Figure 2. Oxidative kinetic chain reaction.

Both thermal analysis and chemiluminescence data support the general mechanism of degradation where the primary alkyl free radicals are propagated through atmospheric oxygen diffusing into the polymer via the formation of peroxy and hydroperoxy free radicals (Figure 2). In this regard, the action of the phenolic antioxidant is mainly that of a hydrogen donor in eliminating organic free radicals, hence being sacrificially consumed in the process.

Catastrophic failures have been reported during the PP shelf life storage period. Intense investigation has come to the following hypothesis that long lived free radicals trapped in the crystalline domains slowly migrate towards the crystalline/amorphous interface where they react with available oxygen to form peroxy and hydroperoxy radicals and initiate degradation near the interface.[2-4] When sufficient number of the tie molecules between crystallites are cut through this chain scission process, the elongation of the PP is reduced dramatically and catastrophic failures follow.

To confirm that long lived free radicals do play a significant role in the post irradiation PP degradation, a PP film sample was examined by electron paramagnetic resonance (EPR) spectroscopy. A distinct free radical spectra, indicative of the “living” free radical reaction was detected 6 months after an irradiation dose of 25 KGy at a rate of about 10 KGy/hr. This finding confirms the long held view that the free radical mediated oxidative degradation continues in polypropylenes long after the irradiation event. Incidentally, the strong EPR signal was completely eliminated when the sample was annealed in a vacuum oven at 90°C, a temperature much about the glass transition for the amorphous phase for PP, and well into the alpha relaxation (T_m) for the crystalline phase of PP.

It is therefore imperative to develop a rapid testing method where physical degradation of film properties after radiation sterilization can be assessed. Since many of the shipping protocols involve winter shipping simulation, where temperatures approaching freezing are frequently encountered, an ASTM low temperature condition would be required. In order to avoid large numbers of samples of actual packaging to be tested, it was decided a film testing methodology be employed. By quantitatively monitoring the real time high speed stress strain behavior under various temperatures, a better understanding on the material behavior can be obtained and a predictive correlation with actual packaging achieved.

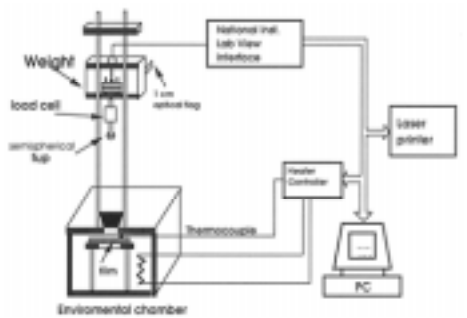

Figure 3. Instrumented impact tester.

RESULTS AND DISCUSSION

A custom designed instrumented impact tester (Figure 3) was constructed based on the load frame of a Dynatup® drop weight impact tester.

HARDWARE DESCRIPTION

An environmental chamber was fitted to the bottom of the impact tower with an opening for the instrumented tup to pass through. An insulating cover is placed on the opening and removed just prior to the release of the weighted tup. A 15 cm circular film holder modeled after an embroidery hoop was constructed with aluminum with an "O-ring" groove containing a Viton® O-ring to elevate the taut film above the inner diameter edge of the holder. In this way, the film is prevented from contacting the relatively sharp radius of the holder and more reproducible data obtained. A multi-sample rack was also constructed so several films can be conditioned in the environmental chamber simultaneously. Temperature control was implemented with a proportional digital temperature controller with a type J thermocouple directly touching the film being tested.

Subambient cooling was achieved with liquid nitrogen feeding from a 100 liter dewar through a throttling valve directly into the environmental chamber. In conjunction with the digital temperature controller, temperatures as low as -150°C can be obtained. The mass of the traveling carriage with the impact tup was adjusted and, depending on the drop height, a minimum available kinetic energy of about 30 J was maintained. An optical flag 1.0 cm in width was attached to the drop weight carriage and the tup velocity just prior to impact measured with an optical gate. Typically, impact velocity of about 3 meters per second was used.

SOFTWARE IMPLEMENTATION

All aspects of data acquisition, user dialog, impact energy calculations, temperature control, and data presentation and archiving were handled by a Lab-View® virtual instrument program by National Instruments on a personal computer. The software was constructed in a modular form to facilitate documentation and validation. Briefly, each one of the modules are described below:

(1) Temperature control: a digital temperature controller using an Iron Constantan (Type J) thermocouple with an RS-232 interface was used to control temperature and communicate with the main program.

(2) Velocity sensing: the transit time for the 1.0 cm aluminum optical flag through an optical gate is measured by a timer function on the National Instruments digital I/O board on the personal computer.

(3) High speed force sensing: the strain gage output from the impact head is first conditioned by an instrumentation amplifier before conversion by a high speed analog/digital converter on the National Instruments interface board at up to 20,000 conversions/second 50μ second / datapoint).

(4) Energy integration: the impact force is integrated against displacement (converted from tup velocity) to obtain the impact energy as a function of displacement, and plotted on a dual vertical axes on the graphical presentation. A typical graphical display is shown in Figure 4.

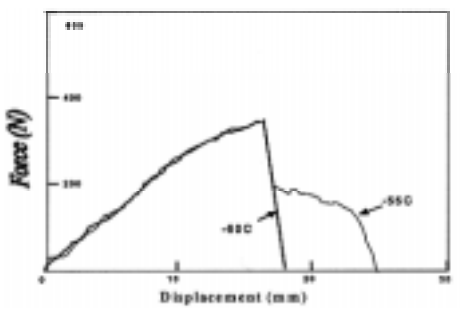

Figure 4: Sample film impact data at two temperatures.

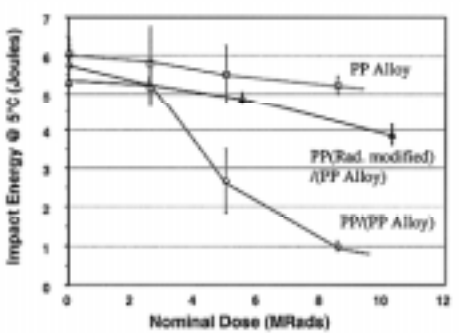

Figure 5. PP films - impact energies vs. dose.

EXPERIMENTAL DESIGN

Three films were selected for low-temperature impact testing: a PP alloy film, a multi-layer film containing the same PP alloy, but with a thin PP layer (about 10% of overall thickness), and a multi-layer film consisting of the same PP alloy and thickness ratio, but with a modified PP layer. The modification of the film construction was the incorporation of a small amount of elastomeric impact modifiers[5] into the PP layer, resulting in a "toughened" film. The three films were sterilized at three radiation dosages: 20, 50 and 90 KGys (± 10 KGys). Samples from each dose (including control) were impact tested to determine the effect of the modification. The samples were tested at 5°C with a falling weight of 5.77 Kg at a velocity of roughly 3 m/s. The resulting morphologies and impact energies were compared to determine any differences between the films.

IMPACT DATA

Integrated impact energy data for each film is plotted as a function of radiation dose in Figure

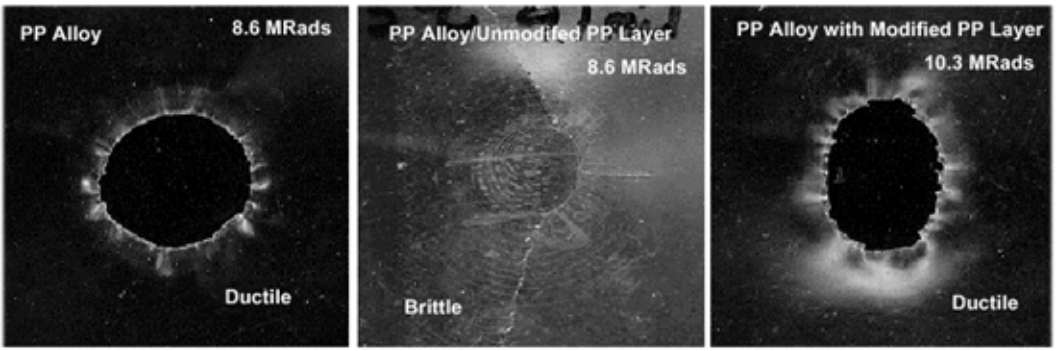

Figure 6. Film impact morphologies.

5. The PP alloy film maintains almost 90% of its impact energy over the range of radiation dosages with no morphological changes. The multilayer film with the unmodified polypropylene layer suffered a dramatic loss in ductility above 2 MRad (or 20 Kgy). By examining the impact energy and morphology of the PP alloy, it is evident that the addition of the PP layer has significantly reduced the impact energy. In addition, the failure morphology of the PP alloy/unmodified PP layer film had transformed from ductile to brittle. Although the bulk of the film layers are quite ductile, the film as a whole is brittle. This is another one of the classic cases where in a multilayer construction, the overall material ductility is governed by the brittle layer. Evidently, when the brittle layer fails, sharp cracks are created in a very short time. At the tip of these cracks very high stress concentrations are localized which lead to very high effective strain rates of loading. Under these high strain rates and highly concentrated local stresses, brittle failures are propagated through the ductile layers.

As the data in Figure 5 indicates, the impact energy for the multilayer film with the modified PP layer remained high up to 80 KGy, the upper limit of our experiment. More importantly, the failure morphology remained ductile throughout all dose conditions. Figure 6 shows the different morphologies observed between the PP alloy, the unmodified multilayer film and the modified multilayer film.

SUMMARY AND CONCLUSIONS

Three films were evaluated by impact testing at 5°C to assess the physical degradation after radiation sterilization. The films were selected to examine the relationship of a PP layer when modified with the addition of elastomeric impact modifiers. The morphologies and impact energies were examined. It was found that the addition of a PP layer, contributing as little as 10% to the overall thickness of a film, reduces the impact energy significantly and

changes the morphology from a ductile fracture to a brittle fracture. However, with the addition of the impact modifying elastomer, the film can maintain close to 90% of its original impact strength and remain ductile.

REFERENCES

1 K. Gillen and R. Clough, in **Irradiation Effects on Polymers**. D. W. Clegg and A. A Collyer, Eds., *Elsevier Applied Science*, New York.
2 R. J. Rolando, "Radiation Resistant Polypropylene: New Development," *J. Plastic Film & Sheeting*, **9**, (4), 326. 1993.
3 L. Woo, J. Palomo, T.K. Ling, E. Chan and C. Sandford, "Shelf-Life Prediction Methods and Applications," *Medical Plastics and Biomaterials*, **3**, (2), 36. 1996.
4 G. Herbert, "The Effect of Molecular Orientation on the Radiation Stability of Polypropylene", *Medical Plastics and Biomaterials*, **3**, #3, 40-43. 1998.
5 N. R. Legge, G. Holden, and H. E. Schroeder, eds. **Thermoplastic Elastomers**. *Hanser Macmillan*, New York. 1987.

Aspects of the Tensile Response of Random Continuous Glass/Epoxy Composites

Okenwa I. Okoli, G.F. Smith
Warwick Manufacturing Group, University of Warwick, Coventry CV4 7AL

INTRODUCTION

The automobile sector continues to provide significant growth opportunities for polymer composites. Although it is recognized that the growth of plastics consumption in cars in the nineties will be evolutionary rather than revolutionary, there is no doubt that the well proven advantages of polymer composites such as weight savings, corrosion resistance and functional integration are more important than ever for the industry.[1] Nevertheless, fibre reinforced composites (FRC) are still regarded as relatively new materials within the mechanical engineering field and often lack the detailed material property data associated with metals. In particular, the use of composites in safety critical applications, leads to uneasiness since the mechanical response in crash applications is not well understood.[2]

The need for a full characterization of the behavior of fibre reinforced polymer composites under dynamic loading conditions has prompted numerous investigations in recent years.[2-12] However, when compared to metals, relatively few studies have been conducted to investigate polymer mechanical properties at high strain rate.[13] In addition, the increasing use of fibre reinforced composites has prompted the need to ascertain the fibre contents necessary to provide the essential mechanical properties. In safety critical applications, it is therefor necessary to investigate the effect of increasing fibre content on the energy released or absorbed by the structure.

This work set out to investigate the effect of strain rate on failure mechanisms and that of fibre content on energy absorption in random continuous glass/epoxy composites.

EXPERIMENTAL WORK

Two materials were tested. The first was a 3 mm thick random continuous glass/epoxy Von Roll Isola composite laminate. The composite had a fibre weight fraction of 65%. The second material were locally manufactured (W.M.G.) random continuous laminates with different fibre volume fractions (15.5, 20.7, 26.9, 38.0 and 41.2%).

The apparatus and procedure used to obtain the tensile properties have been described elsewhere.[2]

RESULTS AND DISCUSSION

EFFECT OF STRAIN RATE ON FAILURE MECHANISMS

The failure mechanisms will be discussed with the aid of photomicrographs.

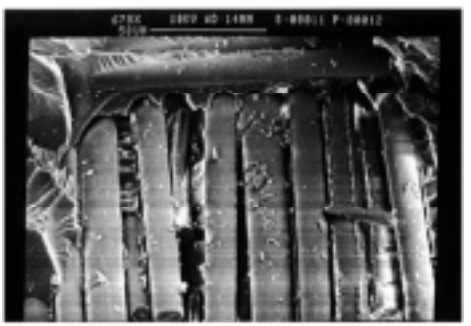

Figure 1. Von Roll Isola Grade 68.660 Laminate showing fibre-matrix debonding (x678).

Figure 1 shows a magnified (x 678) fracture surface of a 68.660 laminate tested in tension at a cross-head rate of 1.7×10^{-2} mm s^{-1}. Fracture is in the direction parallel to fibre reinforcement and as such, distinct river marks can be observed, indicating the direction of crack propagation. These river marks correspond to fracture ridges formed by minutely displaced failure planes.[14]

There is little evidence of fibre-matrix adhesion, which suggests a poor interfacial bond. This results in the gaps observed at the attached ends of the fibres, and the long fibre pull-outs and indicates composite toughness. However, the visible fibre ends indicate brittle failure in the fibres.

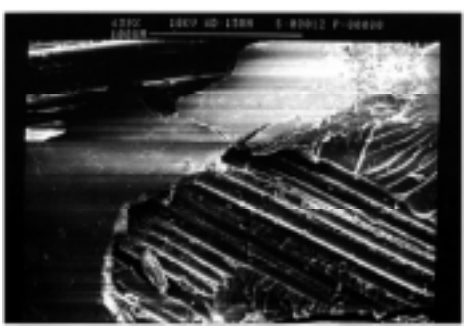

Figure 2. Von Roll Isola Grade 68.660 Laminate showing catastrophic failure in matrix with signs of delamination and fibre pull-out (x439).

Figure 2 shows a magnified (x 439) fracture surface of a 68.660 laminate tested in tension at a cross-head rate of 83×10^{-2} mm s^{-1}. Catastrophic failure in the matrix with signs of delamination and fibre pull-out can be observed. Catastrophic failure, as reported by Broutman[15] is typical in cases of low levels of adhesion in the fibre-matrix interface. This kind of failure results in high energy absorption, with the occurrence of multiple delaminations and does not allow for significant fibre failure. However, the increase in tensile strength at this loading rate (see Table 1), is due to the increased strength of the glass fibres with strain rate. It has been demonstrated, that the tensile modulus of elasticity,[16] and tensile strength,[17] of glass fibres increases with strain rate. It then follows that the observed rate dependence of the failure strength follows from the increased strength of the glass fibres. In consequence,[3] the energy

involved in the failure of the FRC specimens as determined from the area under the stress-strain curve, increases with strain rate. River marks are also visible, showing the direction of crack propagation in the matrix.

Table 1. Tensile property data of 3 mm thick Von Roll Isola grade 68.660 glass/ epoxy laminates at low strain rates

Cross-head, mm s^{-1} ($x10^{-2}$)	Tensile, MPa	Strain rate, s^{-1} ($x10^{-3}$)	Log of strain rate, s^{-1}
1.7	280	14.8	-3.8300
8.3	301	73.2	-3.1357
17.0	304	100.0	-3.0000
83.0	318	700.0	-2.1549

Table 2 The energy to failure of the W.M.G. manufactured random continuous Glass/Epoxy composite laminates obtained at different % fibre volume fractions

Volume Fraction (%)	15.5	20.7	26.9	38.0	41.2
Energy (J)	1.641	6.306	7.438	5.254	5.251

EFFECTS OF FIBRE VOLUME FRACTION ON ENERGY ABSORPTION

The energy to failure of the random continuous (W.M.G.) laminates obtained at different fibre volume fractions is presented in Table 2. Figure 3 shows the variation of expended energy with fibre volume fraction. The relationship is non-linear, with considerable scatter in the data. Expended energy was found to increase to a peak value, then decrease as fibre volume fraction was increased. This behavior, can be attributed to the failure modes of the composite laminates. It was reported,[18] that impact energy increases with fibre volume fraction. However, increasing the fibre content decreases the volume of matrix between fibres, and reduces the inter-laminar strength of the composite.[19]

Figure 4 shows a magnified (x750) fracture surface of an W.M.G. laminate with 41.2% fibre volume fraction tested in tension at a cross-head velocity of $83x10^{-2}$ mm s^{-1}. It was reported[20] that composites with fibre volume fractions (40-50%) commonly exhibit brittle failure with fibre pull-out. This trend can be observed in the Figure 4. The broken fibre ends are flat indicating brittle failure, and signs of fibre pull-out can be found in the matrix. Traces of matrix adhesion can be observed on the fibres. Agarwal and Broutman[20] reported

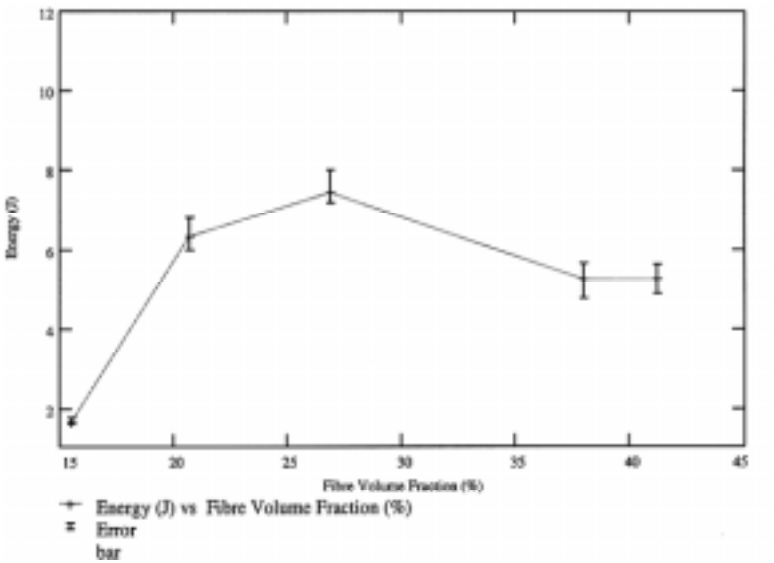

Figure 3. Expended Energy variation of the W.M.G. manufactured random continuous glass/epoxy composite laminates with % fibre volume fraction.

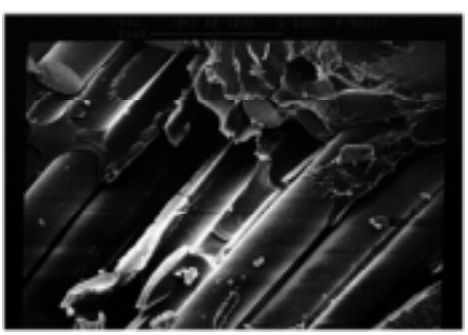

Figure 4. W.M.G. Random continuous glass/epoxy laminates with 41.2% fibre volume fraction showing matrix exhibiting signs of fibre pull-out and fibres showing little matrix adhesion (x750).

that initiation energy increases with interface strength. This may be applied to the present situation where interface strength has fallen due to increased fibre volume fraction with a resultant fall in energy.

CONCLUSIONS

The random continuous (Von Roll Isola 68.660) laminates showed low levels of fibre-matrix interfacial bonding bringing about the long fibre pull-outs observed. This resulted in catastrophic failure with increase in test speed. The foregoing suggests that although the fibres fail in a brittle mode, the matrix failure mode is dominant. In addition, increasing the test speed results in catastrophic failure due to enhanced crack propagation rate and an increase in fibre tensile strength.

The effects of fibre volume fraction on expended energy were studied for random continuous (W.M.G.) laminates. Energy was found to increase to a peak value with increasing

fibre volume fraction to an optimum value (26.9%) after which further increase in the volume fraction brought about a decrease in energy. The point above which increasing the fibre volume fraction becomes detrimental to energy absorption is considered to be where the flowability (measure of the extent to which the movement of the resin is allowed to fill all parts of the mould) of resin is restricted by the glass fibres resulting in poor wetting and consequently, poor fibre-matrix interfacial bonding.

REFERENCES

1 M. Sönmez, **Plastics Consumption in Automotive Applications**, in Automotive Manufacturing International, *Sterling Pub. Grp*., 1993, (pp. 210-214).

2 O.I. Okoli, G.F. Smith, Overcoming Inertial Problems in the High Strain Rate Testing of a Glass/Epoxy Composite. Proceedings of Society of Plastics Engineers Annual Technical Conference, Advanced Polymer Composites Div., Vol. 2, ANTEC, May 1995, (pp. 2998-3002).

3 J. Harding, L.M. Welsh, A Tensile Testing Technique for Fibre-Reinforced Composites at Impact Rates of Strain. *J. Materials Science*, Vol. **18**, 1983, (pp. 1810- 1826).

4 A.M. El-Habak, Effect of Impact Perforation Load on GFRP Composites. *Composites*, Vol. **24**, No. 4, 1993, (pp.341-345).

5 D. Delfosse, G. Pageau, R. Bennett, A. Poursartip, Instrumented Impact Testing at High Velocities. *Journal of Composites Technology and Research*, JCTRER, Vol. **15**, No.1, 1993, (pp. 38-45).

6 A.M.A. El-Habak, Compressive Resistance of Unidirectional GFRP Under High Rate of Loading, J*ournal of Composites Technology and Research*, JCTRER, Vol. **15**, No.4, 1993, (pp. 311-317).

7 O.I. Okoli, High Speed Performance of Composite Materials, in Engineering Polymers Integrated Capability (EPIC) Conference, work area 2d, University of Warwick, UK, March 1996.

8 O.I. Okoli, A. Abdul-Latif, G.F. Smith, The Impact Response of Glass Fibre Reinforced Composites: A Comparison Between Finite Element Results and Experimental Data. Proceedings of Society of Plastics Engineers Annual Technical Conference, Advanced Polymer Composites Division, Vol. 2, ANTEC, May 1996, (pp. 2504- 2509).

9 O.I. Okoli, G.F. Smith, The Effects of Strain Rate on the Failure Energy of Fibre Reinforced Composites. Proceedings of the First International Conference on Composite Science and Technology, Durban, South Africa, June 1996, (p. 359).

10 G. Zhou, Characteristics of Impact Energy Absorption During Damage Development in Laminated Composites. Proceedings of the 4th International Conference on Deformation and Fracture of Composites, Manchester, Institute of Materials, March 1997, (pp. 55-68).

11 O.I. Okoli, G.F. Smith, The Effects of Strain Rate and Fibre Volume Fraction on the Failure Modes of Fibre Reinforced Composites. Proceedings of the 4th International Conference on Deformation and Fracture of Composites, Manchester, Institute of Materials, March 1997, (pp. 77-88).

12 O.I. Okoli, G.F. Smith, Semi-Empirical Relation for the Determination of Dynamic Young's Modulus in Woven Glass/ Epoxy Reinforced Composites. Proceedings of Society of Plastics Engineers Annual Technical Conference, Advanced Polymer Composites Division, Vol. 2, ANTEC, April 1997, (pp. 2373-2376).

13 S.M. Walley, J.E. Field, P.H. Pope, N.A. Safford, The Rapid Deformation behavior of Various Polymers. *J. Physics III France*, **1**, 1991, (pp. 1889-1925).

14 B.W. Smith, Fractography for Continuous Fibre Composites, in **Engineered Materials Handbook: Composites**, Vol. 1, 1989, (pp. 786-797).

15 P. Yeung, L.J. Broutman, The Effect of Glass-Resin Interface Strength of Fibre Reinforced Plastics. *Polymer Engineering and Science*, 1978, Vol. **18**, PT. 2, (pp. 62- 72).

16 A.E. Armenàkas, C.A. Sciammarella, *R*esponse of Glass-Fibre-Reinforced Epoxy Specimens to High Rates of Tensile Loading. Experimental Mechanics, October 1973, Vol 13, (pp. 433-440).

17 L. M. Welsh, J. Harding, Dynamic Tensile Response of Unidirectionally- Reinforced Carbon Epoxy and Glass Epoxy Composites. Proc. 5th Int. Conf. On Composite Materials ICCM V, TMS-AIME,1985, (pp. 1517- 1531).

18 P.K. Mallick, **Fibre-Reinforced Composites: Materials, Manufacturing, and Design**, *Marcel Dekker Inc*., New York and Basel.

19 G.L. Farley, R.K. Bird, J.T. Modlin, The Role of Fibre and Matrix in Crash Energy Absorption of Composite Materials. Proc. American Helicopter Society, National Specialists' Meeting, Crashworthiness Design of Rotor Craft, 1986.
20 B.D. Agarwal, L.J. Broutman, **Analysis and Performance of Fibre Composites**. 2nd ed., 1990, *John Wiley and Sons, Inc.*, New York.

Comparing the Long Term Behavior of Tough Polyethylenes by Craze Testing

KC Pandya and JG Williams
Department of Mechanical Engineering, Imperial College, London, UK

INTRODUCTION

The time dependent nature of the mechanical properties of polyethylene has been the cause of a number of field failures in commercial pipelines and has been investigated by a number of workers.[1-3] Such failures normally occur through the development of long term slow crack growth mechanisms in pipes subject to some form of constant loading during service. Estimating the lifetime of existing pipes and increasing the slow crack growth resistance of new pipelines requires a proper understanding of the structure–property relations that govern the initiation of slow crack growth. This can then be used to improve cost effectiveness by maximizing durability and minimizing the need for replacement.

Near the crack tip, under the effect of a high local triaxial stress state, small microvoids may open up and subsequently grow in size and coalesce. A fully formed craze consists of a network of large coalesced voids interspersed between fibrils which are highly orientated in the stress direction. It is now well established that crazing is the precursor to slow crack growth in polyethylene[2,4] and that the nature of the separation processes that lead to the breakdown of the craze governs the resistance of the material to slow crack growth.

The appropriateness of the choice of experimental method and means of analysis depends on the inherent properties of the material under investigation. In low and medium toughness grades of polyethylene the craze zone may be contained within a K or J dominant stress field allowing conventional fracture mechanics to be used. With increasing optimization of structural properties such as molecular weight and distribution of short chain branches in the toughest grades of polyethylene, a substantial craze zone forms ahead of the crack tip invalidating the use of a single parameter fracture criterion.

A new method of craze analysis is presented here using high constraint circumferentially deep notched tensile (CDNT) specimens.[5,7] The notion behind the test is that when a specimen is loaded in tension, the deep symmetrical notches develop a highly constrained region within the confined ligament which cavitates and fails thus replicating the worst case damage mechanisms seen in polyethylene pipe in the field. The method involves measuring

the local separation properties of a craze under both constant load and constant speed conditions and quantifying the long term behavior of different grades of tough polyethylene on this basis. Focussing in this way specifically on the local decohesion within the fracture process zone represents an important departure from mainstream fracture methods that may seek instead to accommodate crazing within a continuum analysis.

In recent times a lot of research has been carried out on the analysis of interfacial decohesion through the development of cohesive zone modelling techniques.[6] The basis of this method lies in characterizing crack growth in a material through the specification of a local fracture criterion which relates cohesive stresses to separation at an interface. Experimentally measured rate dependent traction – separation curves presented in this paper represent an example of such a criterion. The curves contain all the necessary information pertaining to load transfer and energy consumption mechanisms within the craze and in principle may be applied to the general problem of interfacial decohesion in polyethylene in any geometry under a variety of loading conditions.

TEST PROCEDURE AND SPECIFICATIONS

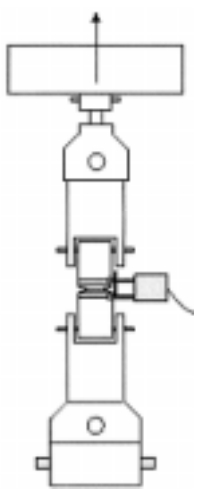

Figure 1. Test Procedure under constant speed conditions.

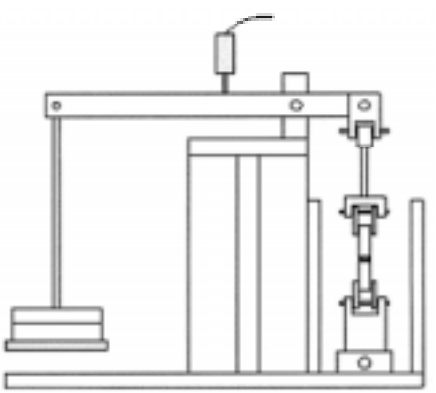

Figure 2. Test Procedure under constant load conditions.

Rectangular specimen blanks were cut from compression moulded plaques supplied by BP Chemicals, placed in a four jaw self centring chuck and notched on a lathe using a single point notching tool. The circumferential notch was then sharpened with a new razor blade. The geometrical specifications of the notched specimens are as follows:

L x B x W: 120 x 16 x 16 mm

Ratio of ligament to bulk cross sectional area: 1/10

Angle of notching tool: 19^{o}

The experimental apparatus for tests under constant speed conditions is shown in Figure 1. The specimens were tested on an Instron machine with an extensometer mounted on the specimen to measure the craze extension as the test proceeded. Load was measured by a load cell and the load time trace recorded. Tests were run over a speed range of 50.0 mm/min to 0.005 mm/min. The experimental apparatus for

Table 1. Selected structural properties of the test materials

Material	Density, kg/m^3	M_w, g/mol	Comonomer/1000C
PEI	940	185,000	4.5
PEII	947	310,000	2.5
PEIII	947	290,000	1.5
PEIV	954	355,000	0.0

tests under constant load conditions is shown in Figure 2. The total extension was measured using a linear voltage displacement transducer from which the craze separation was obtained by correcting for the bulk extension of the specimen. A data logging system was used to record the extension as a function of time as the test proceeded. The grades of polyethylene under investigation are shown in Table 1. PEI and PEII are members of the commonly used generic group of polyethylenes of PE80 and PE100 respectively. PEIII and PEIV are an experimental copolymer and homopolymer respectively.

TEST RESULTS

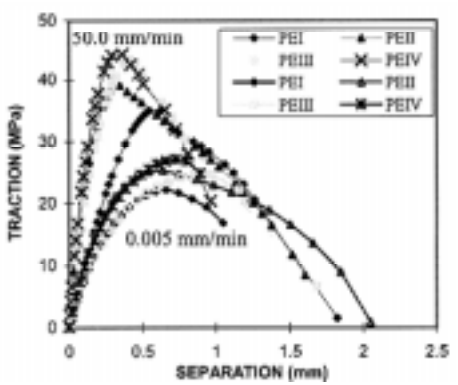

Figure 3. Comparison of traction - separation curves.

At constant speed, the interfacial holding traction, which is defined using the original ligament area, is seen to vary as the test proceeds, rising from zero along the so called cohesion branch of the traction – separation curve to a maximum value and then falling to zero again along the decohesion branch as the craze surfaces separate. The curve is governed by two properties, the craze (maximum) stress and the break separation which together with the shape of the curve define the work of separation (γ). Variations in the structural properties of the test materials and the nature of their rate dependence are reflected in the differences in the values of these properties and in the general shapes of the curves.[7]

Traction – separation curves at a speed of 50.0 mm/min and 0.005 mm/min for the four grades of polyethylene shown in Table 1 are compared in Figure 3. For PEI, PEIII and PEIV differences in the shape of the traction – separation curve at high and low speeds indicate a transition from ductile behavior at high speeds to macroscopically brittle behavior at low

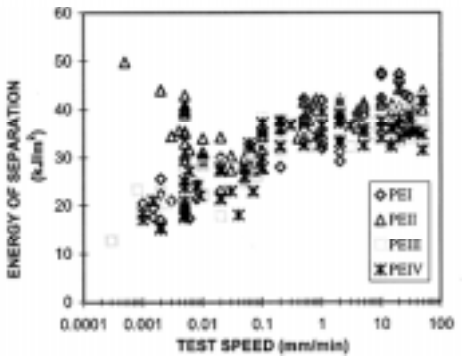

Figure 4. Comparison of energy - time behavior.

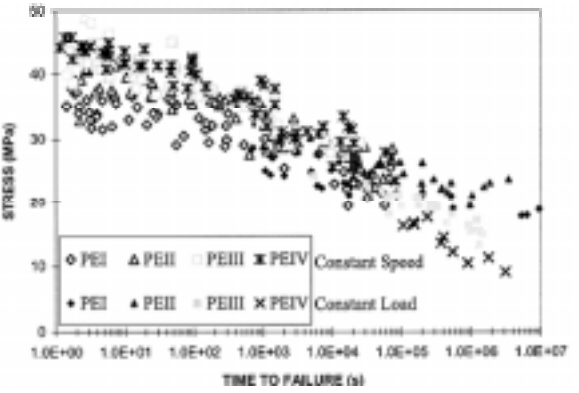

Figure 5. Stress - time behavior under constant load and constant speed conditions.

speeds, shown by the much lower value of γ. However the behavior of PEII differs from the other grades at low speeds. This is more clearly seen if γ (the area under the traction - separation curve) is plotted as a function of test speed as shown in Figure 4 and indicates the behavior of PEII at low speeds of a rising energy of separation with falling test speed.

The long term behavior of the grades can be analysed under constant load conditions by plotting the net section stress as a function of time to failure. Each grade of polyethylene is seen to have a specific stress – time dependence, with variations in the trends related directly to differences in the structural properties. Figure 5 combines the craze stress obtained under constant speed conditions with the net section stress obtained under constant load conditions as a function of time to failure for each grade. Doing so allows the behavior of each grade to be mapped over failure times ranging from seconds to weeks and for comparisons to be made between the performance of each grade under different loading conditions. There is a clear trend of falling stress with falling test speed under constant speed conditions and with falling load under constant load conditions.

DISCUSSION OF RESULTS

In Figure 3 at 50.0 mm/min the break separation for PEI, PEII and PEIII are comparable while the value is much lower for PEIV. In general, for the same test speed craze stress falls with falling density. This may be explained in the following way. Crazing is a voiding and cavitation process. Given that we take the material in each grade to be homogenous prior to craze development the question arises as to where the microvoids nucleate. A possible answer lies in the degree of free volume that is available within a material. A low density

material is likely to have a higher percentage of free volume than a high density material due to the difference in the degree of packing of the molecular chains. Consequently the stress required to produce a craze is much lower in PEI than PEIV.

The curves at 0.005 mm/min in Figure 3 demonstrate the effectiveness of the test method in being able to differentiate between the behavior of each grade in the quasi-static speed range. The craze stress again follows the changes in density. However, in contrast to the high speed tests, the decohesion behavior of each grade at low speeds is dependent more on the structural properties of the molecular chain rather than the density such that differences in the values of break separation between the grades are.greater than at high speeds. PEII has a much higher break extension than the other grades at 0.005 mm/min. Consequently the energy of separation at this speed for PEII is twice that for the other copolymers. It seems that the optimization of the high molecular weight and appropriate chain branching in PEII results in it having the highest break separation. A large amount of energy is thus needed for chains to overcome secondary forces and slip past each other. The disentanglement processes that precede craze breakdown are thus greatly inhibited. In contrast, in the homopolymer PEIV, the extent of stable craze growth is extremely limited indicating the ease of disentanglement of a smooth molecule. Given the high molecular weight of PEIV this also indicates the greater importance of short chain branching over molecular entanglements in inhibiting craze breakdown.

The trends for energy of separation as a function of test speed are compared for each grade in Figure 4. PEII occupies an upper energy band across the intermediate and low speed range. All four grades seem to show a high speed (50.0 mm/min to 1.0 mm/min) plateau region. Such high energy ductile failure is accompanied by the formation of a small number of large voids, the growth of which results in a decrease in stress transfer and high energy of separation. A transition occurs in the behavior for all grades at around 0.1 mm/min. At speeds lower than this PEI, PEIII and PEIV show a decreasing energy of separation with falling test speed. However, for PEII at low test speeds, the energy value rises with falling test speed, governed in the main by rising break separation as was seen earlier in Figure 3. Such behavior is quite contrary to the more generally expected low speed, macroscopically brittle behavior shown by the others. Understanding this behavior has important implications for the development of materials with long term resistance to slow crack growth mechanisms.

Stress - time data obtained under constant speed and constant load conditions are shown in Figure 5. The two loading conditions do not predict the same ranking of the grades. For example, choosing time to failure as the criterion for assessment, at a stress of 40 MPa using the constant speed data the grades are ranked in order of descending toughness as PEIV, PEIII, PEII and PEI. However, at 20 MPa using the constant load data the

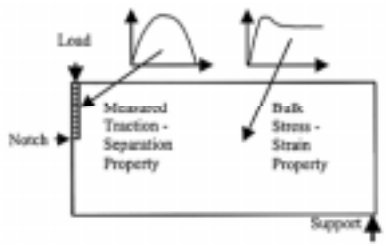

Figure 6. Application of measured craze properties to a cohesive zone model using a three point bend geometry.

ranking in order of descending toughness is PEII, PEI, PEIII and PEIV. The short term constant speed data reflect the differences in densities of the grades while the long term constant load data are affected more by differences in molecular weight and branch chain density. It is also clear, bearing in mind the results of the energy - speed behavior in Figure 4, that the mapping of stress - time behavior alone does not provide sufficient information for the assessment of toughness.

APPLICATION OF RESULTS TO COHESIVE ZONE MODEL

A predictive 'cohesive zone' type fracture model is introduced based on the 'Finite Volume' method which incorporates the measured traction - separation curve as a local fracture criterion.[7,8] A three point bend specimen is taken as an illustrative example as shown in Figure 6, where using geometrical symmetry only half the specimen is modelled. A measured traction - separation curve is specified along the plane of symmetry and governs the opening of the craze surfaces. Bulk stress-strain properties obtained experimentally from standard plane stress dog bone specimens are also specified. The central premise of this approach is that the measured traction curves are a material property and can be used to model decohesion in any physical situation for a given rate and temperature.

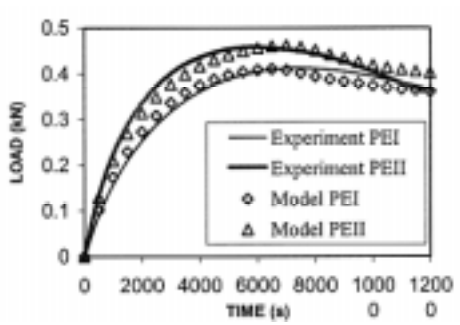

Figure 7. Comparison of experimental and predicted load - time curves in a three point bend geometry.

Experiments were run at slow rates on three point bend specimens for PEI and PEII. Model predictions of load - time behavior and crack growth from numerical simulations of the three point bend specimens have been found to agree very well with experimental results as shown in Figure 7 for tests run at 0.1 mm/min. This is potentially a powerful method given that the fracture model is based on the mechanics of craze separation, the physical basis of which has been experimentally verified. The prediction of failure through the examination of interfacial decohesion would mean that it should be applicable to many different physical situations. There thus appears to be considerable scope for extending this method to other geometries, including pipe geometries, and other loading conditions in order to obtain quantitative predictions of the initiation of slow crack growth in tough polyethylenes.

CONCLUSIONS

Circumferentially deep notched tensile specimens were used successfully to assess the behavior of tough polyethylenes on the basis of their craze mechanics under constant speed and constant load conditions. Experimentally measured traction - separation curves under constant speed conditions were shown to provide good discrimination between the grades and highlighted the superior toughness of a particular grade of PE100. Results under constant load conditions provided a useful stress - time characterization of the grades and also highlighted in general the inferior performance of homopolymers compared to copolymers. A means of further analysis was introduced by applying measured traction - separation curves to a cohesive zone model. Experimental and numerical results have been found to be in excellent agreement. This indicates the possibility of applying the model to a range of fracture problems including the prediction of the initiation and growth of slow cracks in pipes.

ACKNOWLEDGEMENT

The authors thank BP Chemicals for supplying the test materials and for their financial support of this research project. Thanks is also due to Dr. Ivankovic of Imperial College for his advice on the numerical model.

REFERENCES

1 Chan M.K.V., Williams J.G., "Slow Stable Crack Growth in High Density Polyethylenes", *Polymer*, **24**, (1983) p. 234 – 244

2 Bhattacharya S.K., Brown N., "The Initiation of Crack Growth in Linear Polyethylene", *J. Mater. Sci*., **20**, (1985) p. 2767 – 2775

3 Egan B.J., Delatycki O., "The Morphology, Chain Structure and Fracture Behavior of High-Density Polyethylene", *J. Mater. Sci*., **30**, (1995) p. 3307 – 3318

4 Friedrich K., "Crazing and Shear Bands in Semi-Crystalline Thermoplastics", *Adv. Polym. Sci*., **52/53**, (1983) p. 225–274

5 Duan D., Williams J.G., "Craze Testing for Tough Polyethylenes", *J. Mater. Sci*., **33**, (1998) p. 625 - 638

6 Needleman A., "An Analysis of Decohesion along an Imperfect Interface", *Int. J. Fract*., **42**, (1990) p. 21 - 40

7 Pandya K.C., Williams J.G., "Measurement of Cohesive Zone Parameters in Tough Polyethylene", *Polym. Eng. Sci*., submitted for publication.

8 Pandya K.C., Ivankovic A., Williams J.G., "Predicting Crack Growth in Tough Polyethylene from Measured Cohesive Zone Traction - Separation Curves", 11th International Conference on Deformation, Yield and Fracture of Polymers, (2000) abstract submitted.